Forecasting microcystin concentrations in Lake Erie using an eulerian tracer model

Xing Zhou[a, b], Justin D. Chaffin[c], John F. Bratton[d], Edward M. Verhamme[d], Pengfei Xue[a, b, e] *

[a]Department of Civil, Environmental and Geospatial Engineering, Michigan Technological University, 1400 Townsend Dr., Houghton, MI 49931, USA

[b]Great Lakes Research Center, Michigan Technological University, 1400 Townsend Dr., Houghton, MI 49931, USA

[c]F.T. Stone Laboratory and Ohio Sea Grant, The Ohio State University, 878 Bayview Ave. P.O. Box 119, Put-In-Bay, OH 43456, USA

[d]LimnoTech, 501 Avis Drive, Ann Arbor, MI 48108, USA

[e]Environmental Science Division, Argonne National Laboratory, Lemont, IL 60439, USA

*Corresponding Author: pexue@mtu.edu

Keywords

Cyanobacteria, Cyanotoxins, Eutrophication, Environmental Modeling, *Microcystis*, Harmful Algal Bloom

Abstract

Cyanobacteria biomass models are routinely used in Lake Erie to predict the occurrence and location of algal blooms. However, current forecasts do not predict the microcystin toxins produced by these blooms. In this study, we used an extensive dataset of microcystin concentrations to generate weekly distribution maps in Lake Erie for the summers of 2018 and 2019. Using a 3D Eulerian tracer model (ETM), initialized with these maps, we simulated microcystin transport over 7 days, under two conditions: (1) the initial microcystin is mixed within the surface-mixed layer; (2) the initial microcystin is distributed throughout the entire water column. Two scenarios were tested for each condition: one incorporating microcystin production rates into hydrodynamic transport and one excluding them. Model performance was evaluated against weekly sample data in predicting whether microcystin concentrations surpassed specific thresholds (0.3, 1.0, 5.0, 10.0, and 20.0 µg/L), and in predicting trend directionality over each week. Overall, the ETM with hydrodynamics alone captured the transport of microcystins and predicted microcystin concentrations in 69% of the simulations. Incorporating microcystin production into the model increased the accuracy of forecasts by an additional 10%. Moreover, models with microcystin production successfully predicted microcystin concentrations greater than 5 µg/L during a large bloom, high-microcystin year (2019), while incorrectly forecasting concentrations above 5 µg/L during a small bloom year (2018). With limited data to initialize the ETM, no single model configuration consistently outperformed others. It is necessary to consider the full range of model configurations when utilizing their outputs for making management decisions.

Introduction

Lake Erie, the most productive of the Laurentian Great Lakes, has experienced summertime (July to October) cyanobacterial harmful algal blooms (CHABs) in the past two decades (Stumpf et al., 2012; Bridgeman et al., 2013; Steffen et al., 2014). The re-emergence of CHABs in Lake Erie after a period of decline is primarily linked to excessive nutrient input from non-point agricultural sources (Watson et al., 2016; Martin et al., 2021). The most severe CHABs originate in the shallow western basin of Lake Erie near the mouth of the Maumee River due to its close proximity to nutrient loads and favorable temperature and light climate (Chaffin et al., 2011; Kane et al., 2014). Lake Erie CHABs are dominated by *Microcystis aeruginosa*, a highly buoyant colony-former capable of producing high concentrations of hepatotoxic microcystins (MCs) (Steffen et al., 2014; Harke et al., 2016). While many socioeconomic and ecological problems are associated with CHABs, MC contamination of recreational and drinking waters is the most serious concern. One of the most well-known examples is the "do not drink" advisory issued by the City of Toledo in August 2014, which affected half a million people and lasted for three days (Jetoo et al., 2015), as a result of MC concentrations in tap water that exceeded the World Health Organization guideline of 1 μg/L.

Several short-term forecast models have been developed to predict CHAB biomass, distribution, and transport in Lake Erie. These models aim to provide early information on CHAB biomass for decision support, which can help mitigate negative impacts at drinking water treatment plants and beaches. The models are initialized from satellite images of CHAB biomass (Wynne et al., 2010) and use hydrodynamic conditions predicted by a hydrodynamic model to forecast CHAB transport and determine the bloom location and biomass several days into the future (Wynne et al., 2013; Rowe et al., 2016). These short-term forecast models are developed using either a Lagrangian or an Eulerian approach. For example, the Lake Erie Harmful Algal Bloom Forecast system, maintained by the National Oceanic and Atmospheric Administration (NOAA), employs a three-dimensional (3D) Lagrangian particle tracking model (referred to as the NOAA HAB Tracker; available at https://coastalscience.noaa.gov/research/stressor-impacts-mitigation/hab-forecasts /lake-erie/, accessed December 11th, 2021). This model is used in combination with satellite images to provide information on the bloom's current location and biomass, as well as its forecasted position over the next 96 hours. A 3D Eulerian tracer model has also been tested to predict CHAB biomass distribution and is planned to be linked to the operational version of the Water Cycle Prediction System for the Great Lakes by Environment and Climate Change Canada to produce daily forecasts of CHAB transport (Soontiens et al., 2019).

The Eulerian and Lagrangian approaches differ in how they describe fluid properties, such as toxin concentration, within a field. The Lagrangian approach focuses on tracking the motion of numerous discrete flowing particles and their associated properties as they move through the field. The trajectories and properties of individual particles are changing as they evolve over time. By releasing and observing a multitude of such particles, one can obtain a comprehensive

understanding of the fluid's dynamics and properties in the domain. Conversely, the Eulerian approach adopts a fixed spatial frame of reference, describing the fluid properties at specific, predetermined points within the field. Within this framework, one describes the temporal evolution of fluid properties at a vast array of fixed locations across the domain to understand the flow system. The Eulerian tracer models are more effective in representing continuous concentration fields and is more compatible with lower-food web biological models, which are also developed within the Eulerian framework (Xue et al., 2014; Rowe et al., 2017; Zhou et al. 2023). In contrast, the Lagrangian approach is better suited for representing properties that vary across a population, such as buoyant velocities for *Microcystis* colonies. Moreover, the Lagrangian approach is well-adapted for tracking exposure to environmental conditions over time, which is essential for individual-based models of organisms (Li et al., 2014).

Recently, Zhou et al. (2023) conducted a comprehensive evaluation of Lagrangian and Eulerian transport models for forecasting cyanobacterial harmful algal blooms (CHABs) in Lake Erie. The study compared three types of 3D models: 1) a Lagrangian particle model (LPM), 2) an Eulerian tracer model (ETM), and 3) a property-carrying particle model that utilizes a hybrid Eulerian-Lagrangian approach. The results indicated that all three transport models demonstrated similar levels of skill, with the ETM outperforming the others in the overall evaluation. Consequently, we chose to use the 3D ETM for forecasting microcystin (MC) concentrations in this study. This decision was also based on the fact that the Eulerian approach is more effective at estimating changes in continuous fields of concentration driven by biophysical processes and offers greater flexibility in incorporating numerical descriptions of biological processes.

Compared to forecasting CHAB biomass, predicting MC concentrations is more challenging. There are relatively few observed MC data points (compared to remote sensing biomass data), which creates a barrier for model development, calibration, and evaluation of model performance. CHAB biomass cannot be used as a proxy for MC concentration, and remote sensing cannot detect MCs (Stumpf et al., 2016). To overcome data limitations, recent research has incorporated the MC-to-chlorophyll ratio from grab samples to forecast MC concentrations. They averaged the ratio across all sites for a given date and then multiplied the mean ratio by remote sensing-derived chlorophyll concentrations to back-calculate MC concentration (Liu et al., 2020). Similarly, Qian et al. (2021) used a MC-chlorophyll empirical relationship in a Bayesian hierarchical modeling framework to forecast MC concentrations. This approach allowed Liu et al. (2020) and Qian et al. (2021) to estimate the spatially- and temporally-resolved probability of MC exceeding certain advisory concentrations in the western basin of Lake Erie; however, this approach has limitations. The MC-to-chlorophyll ratio can range from less than 0.05 to greater than 0.50 throughout the western basin on a single day, suggesting that the MC-to-chlorophyll ratio varies as much spatially as it does temporally (Chaffin et al., 2021). Furthermore, the MC-to-chlorophyll approach omits MC data that does not have a paired chlorophyll measurement (such as drinking water intakes). Ideally, MC forecasts should rely on

measured MC concentrations rather than surrogates.

Additionally, when compared to CHAB biomass forecasts, there are other knowledge gaps in developing an MC forecast. The modeling of CHAB biomass (and likely MCs) transport is sensitive to the initial vertical distribution of the bloom. In CHAB biomass forecast modeling, several studies suggest that applying surface chlorophyll concentrations to the surface mixed layer produces the highest accuracy (Rowe et al., 2016; Soontiens et al., 2019). However, it remains unknown whether the same process can be applied to forecasting MCs. Furthermore, current CHAB biomass models and forecasts (i.e., the NOAA HAB Tracker) assume that physical processes such as water currents and wind mixing dominate over biological mechanisms (cell division and death) in explaining short-term bloom location and biomass (Rowe et al., 2016). Nevertheless, a recent report showed that MC production rates decrease throughout the bloom season (Chaffin et al., 2022). Therefore, it is crucial to evaluate the physical processes influencing the accuracy of MC concentration forecasts and understand how incorporating biological processes could improve these forecasts.

In this study, we used a comprehensive dataset of MC concentrations compiled from multiple sources, including university researchers, federal and state agencies, water treatment plant intakes, and citizen scientists. This data was used to create weekly maps of MC concentrations in Lake Erie to initialize an Eulerian tracer model (ETM; see below for the model description), aiming to predict the spatiotemporal patterns of MC during two CHAB seasons in 2018 and 2019. The MC simulations were analyzed with respect to concentration and extent, focusing on the significance of mixing, whether initial microcystin is mixed throughout the entire water column or within the surface-mixed layer, and biological processes, such as incorporating MC production rates. This analysis aimed to explain the short-term variability of MC concentrations.

Method and Materials

Observational data

We requested MC concentration data from all institutions that routinely (weekly to biweekly) collect grab samples from the western basin of Lake Erie. We received data from five sources, totaling 366 data points in 2018 and 655 in 2019 (see Electronic Supplementary Material (ESM) for Data Sources). The institutions that submitted data collected grab samples using different water collection methods (Golnick et al., 2016) and analyzed microcystins (MCs) by enzyme-linked immunosorbent assay (ELISA; Eurofins Abraxis, #520011, Warminster, PA, USA). We did not request MC data analyzed by other analytical methods (i.e., LC-MS or HPLC) due to the inherent differences in these methods (Chaffin et al., 2021). All health standards are based on ELISA data. No attempt was made to normalize data for differences in sampling depth because Golnick et al. (2016) reported no significant differences in chlorophyll-a concentrations among

different water sample collection methods in a side-by-side comparison study. Microcystin concentrations in the western basin can range from less than 0.3 µg/L in the open waters of the western basin to greater than 40 µg/L in Maumee Bay (Chaffin et al., 2021). Collectively, this indicates that the bias introduced by different water sample collection methods is much smaller than the spatial variability of MCs in western Lake Erie. Most organizations reported total MC (as µg/L), but some provided MC data as particulate MC and dissolved MC concentrations (both as µg/L), which we summed to calculate total MC concentration. Grab sample data were binned by week and assigned a common collection date as occurring on Monday. The largest, regular sample collection programs (e.g., NOAA and the University of Toledo) often occurred on Mondays, except due to inclement weather. This was done to generate weekly MC maps using all available data, which served to provide the initial conditions for the ETM to predict the MC concentrations in the following week. It is important to note that the model results on the actual sampling dates were used for model-observation comparisons for accuracy and reliability.

We used remotely sensed algal biomass images (from the NOAA imagery archive) to identify a zero-MC concentration boundary in weekly maps. The zero-MC boundary was defined by the edge of the visible satellite-derived boundary, determined through image classification. We employed the inverse distance weighting (IDW) tool within ArcGIS to create an interpolated raster of MC concentrations (i.e., MC concentration maps) using all collected data, which were used to initialize the ETM. Figure 1 shows an example for August 19th, 2019.

In addition to the weekly datasets mentioned above, a high-spatial-resolution one-day sampling was conducted on August 7th, 2019 (referred to as "HABs Grab," Chaffin et al., 2021). During this event, 172 grab samples were collected, covering an area of 2,270 km2 in the western basin of Lake Erie within a six-hour measurement window (Fig. 1b). The "HABs Grab" provided a high-resolution distribution of MC and served as the best data source for evaluating the impact of hydrodynamic transport on MC spatial variability. On the other hand, consistent weekly sampling of MC concentrations was conducted by the National Oceanic and Atmospheric Administration's Great Lakes Environmental Research Laboratory and the Cooperative Institute for Great Lakes Research (hereafter referred to as “GLERL”) at eight monitoring locations (Fig. 1c). These data were used to evaluate the modeled seven-day forecast performance temporally. The GLERL samples were most consistently collected on Mondays, with data generated from all eight sites during most sampling cruises. More details about the GLERL dataset can be found in the ESM Data Sources.

Note that the zero-MC boundary, identified using image classification, was also validated using data from the "HABs Grab" that showed no detection of MC outside the satellite-derived biomass boundary. The IDW method also worked well for the "HABs Grab" because there were a large number of samples available (172 collected on one day) within the basin. However, the IDW method may have limitations for weeks when only a handful of MC concentrations were

available, which introduced additional uncertainties to the model's initial conditions. Although the IDW method produced interpolated raster values between known sampling points and the zero-MC edge, the model evaluation focused on the area bounded by the GLERL sampling points.

Hydrodynamic model

The Finite Volume Community Ocean Model (FVCOM) is a three-dimensional (3D) hydrodynamic, free-surface, primitive-equation model that solves the integral form of the governing equations on an unstructured, sigma-coordinate mesh (Chen et al., 2003). FVCOM has been applied in many coastal systems characterized by geometric complexity and highly variable flow patterns, including various applications to the Great Lakes (Anderson et al., 2015; Rowe et al., 2016; Xue et al., 2015, 2017, 2022; Huang et al., 2021).

The Lake Erie (LE)-FVCOM employs an unstructured grid mesh composed of 6106 nodes and 11509 elements (Fig. 1d). The mesh has a grid resolution of 2.5 km in the central basin, 1.5 km in the western basin, and 0.5 km in Maumee Bay (western corner of the basin) and the area around islands between the central and western basins. The model is vertically divided into 20 uniform sigma layers that provide vertical resolution ranging from approximately 0.1 m for the shallow areas (≈ 2 m) to approximately 0.5 m for the deep regions (≈ 10 m) in the western basin of Lake Erie. The open boundary conditions consist of primary inflow from the Detroit River and outflow through the Niagara River, with specified hourly water levels using the NOAA gauges at Gibraltar, Michigan (9044020) and Buffalo, New York (9063020). The LE-FVCOM is driven by hourly atmospheric forcing from the High-Resolution Rapid Refresh (HRRR), a cloud-resolving and convection-allowing weather forecast and data assimilation system running in real time at a 3-km grid resolution (Benjamin et al., 2016).

Eulerian tracer model

The ETM was developed from the FVCOM general ecosystem module (GEM), which solves the advection-diffusion equation coupled to biological functions using a finite volume approach. The advective transport and turbulent mixing of microcystin concentration (C) in the ETM were governed by following equation:

$$\frac{\partial C}{\partial t} + u\frac{\partial C}{\partial x} + v\frac{\partial C}{\partial y} + w\frac{\partial C}{\partial z} - \frac{\partial}{\partial z}\left(K_h\frac{\partial C}{\partial z}\right) - F_c + w_b\frac{\partial C}{\partial z} = C_{source} - C_{sink} \quad (1)$$

where *u, v*, and *w* are the *x, y,* and *z* components of the water velocity, K_h is the vertical thermal diffusion coefficient, w_b is the buoyant velocity, F_c is the horizontal diffusion term, and C_{source} and C_{sink} represents the sources (production) and sinks (loss) of C, respectively, due to the biological processes. In this study, the source and sink terms were replaced by an MC production function (described in the following section).

Microcystis regulates the buoyancy of its colonies, with most of them being positively buoyant in Lake Erie (Den Uyl et al., 2021). The competition between algae buoyancy and turbulent mixing is an important factor in the vertical distribution of colonies within the water column. Wind-driven turbulence can mix colonies deeper into the water column, while calm conditions allow them to float back towards the surface (Medrano et al. 2013; Rowe et al., 2016). As the Eulerian approach represents the characteristics of the population mean rather than describing intrapopulation variability, a representative buoyant velocity of 90 µm/s was used in ETM. This value represented the majority (70%) of the measured buoyant velocities based on the frequency distribution histogram of estimated buoyant velocity described in Rowe et al. (2016). Additionally, Zhou et al. (2023) reported a detailed sensitivity analysis (Zhou et al. 2023, Sections 1, 2, and 3 in ESM) of buoyant velocities for the CHAB biomass forecast. They used a high buoyant velocity of 180 µm/s (representing *Microcystis* colonies with large diameters) and non-buoyant velocity cases to compare with the model forecast using a buoyant velocity of 90 µm/s that represented 70% of the measured buoyant velocities based on the frequency distribution histogram. The results confirmed that using a representative buoyant velocity of 90 µm/s provided the best model performance in the sensitivity analysis of buoyant velocities.

Microcystin production function

The changes in MC concentration caused by biological processes during the model simulation were calculated using the following equation.

$$MC_t = e^{\mu \times t + ln(MC_0)} \quad (2)$$

Where $MC_t$and MC_0 are the microcystin concentrations (µg/L) at time t and time 0 (model start time), respectively. t is the simulation time (day). μ is the intracellular microcystin production rate constant (/day). A positive rate indicates a net production of MCs by algal cells, whereas a negative value indicates a net loss of MCs due to degradation. μ values for each week were determined from a microcosm study that quantified MC production biweekly throughout the 2018 and 2019 CHAB seasons (Chaffin et al., 2022) (ESM Table S1). Briefly, μ was quantified for CHAB collected at two sites in the western basin (Maumee Bay and an offshore site) at ambient nutrient and elevated phosphorus and nitrogen conditions and at *in situ* temperature and light conditions (Fig. 1). The "actual" µ might be somewhere in the middle between ambient and elevated conditions. Because the 'actual' μ was not quantified, we used the averaged μ value from the ambient and elevated nutrient conditions for ETM simulations. In addition, we conducted two sensitivity analyses using the lower and higher quartiles from the range of µ values between ambient and elevated nutrient conditions to identify the uncertainty in the MC production rate and the sensitivity of model performance to the MC production rate (ESM Figure S4). We used μ from the site in Maumee Bay for areas within 20 km of the Maumee River mouth and μ from the offshore site to represent the rest of the basin (Fig. 1d). Because μ was measured biweekly, we used the μ value determined closest to the simulation start date.

Initial vertical distribution of microcystins

The short-term forecast of CHAB biomass and MC concentration is sensitive to the initial vertical distribution of CHABs. In the modeling of CHAB biomass forecast, remotely sensed surface chlorophyll concentrations can be used to improve the initial condition of the model by applying it to the surface mixed layer (Rowe et al., 2016; Soontiens et al., 2019; Zhou et al., 2023). However, the MC concentration map generated here is based on in situ data collected from all water layers due to the limited observational data. The best approach to initializing model vertical distribution with limited observations is still unknown, but the desired metric to track is the total mass of toxins in the full water column. Water intakes generally draw in a well-mixed water column sample that is not affected by surface scums. In this study, we tested the performance of the model by initializing the model under two mixing conditions: (1) distributing the initial microcystin from an MC concentration map throughout the entire water column, and (2) distributing the initial microcystin from an MC concentration map within the surface-mixed layer. Following Rowe et al. (2016), we conducted one-dimensional (1D) simulations to estimate the SML depth in 33 selected locations, providing representative coverage of the most common CHAB regions and an additional three stations in the deeper areas. Each 1D simulation was initialized with 1000 neutrally buoyant particles uniformly distributed throughout the water column. The simulation was set to run from 48 hours before the initialization time of each ETM simulation up to the initialization time to allow the particle distribution sufficient time to adapt to the varying diffusivity. The SML depth was then estimated as the depth at which the 1D concentration profile decreased to half the surface concentration and was interpolated spatially to the ETM nodes by the nearest neighbor method (Rowe et al., 2016).

Design of numerical experiments

The numerical experiments were designed in two parts. In the first part, we focused on the specific event of the HABs Grab (a one-day sampling on August 7th, 2019) that had high spatial resolution and coverage of MC measurements during a severe bloom in the western basin. For this event, we conducted two ETM simulations (including or excluding MC production) from July 29th to August 8th to analyze the impact of hydrodynamic transport and MC production on the spatial variability of MCs. We initialized the model with the latest available MC map (on July 29th) before the 2019 HABs Grab. For the ETM simulation including MC production, we used the average of the MC production rates measured for microcosm water collected on July 16th and August 13th for the area within 20 km of the Maumee River mouth. As there was no sampling event for microcosm water at the Maumee Bay site that was close to July 29th, we used the MC production rate measured on microcosm water from the offshore site collected on July 30th for the rest of the basin.

In addition, we conducted a numerical Lagrangian particle tracking experiment to demonstrate the flow patterns that impact the transport of microcystins (MCs) by displaying the trajectories of fluid particles released from five representative regions on July 29th, 2019 (Fig. 3a). For the particle tracking experiments, we randomly released 60,000 particles in the western basin of Lake Erie from 8:00-16:00 on July 29th and tracked them until August 7th. We calculated particle trajectories using 3D flow fields simulated by LE-FVCOM. It is important to note that the objective of the particle tracking experiments was to illustrate the flow patterns and facilitate understanding of the role of hydrodynamic transport in affecting MC distribution; therefore, the particles in the simulation represent flow parcels rather than MC concentration. Spatiotemporal changes in MC concentration were all simulated using the ETM. Particles were randomly released within the water column. Note that we did not incorporate the random-walk process into the particle tracking, and therefore the turbulent mixing processes were not represented in the particle tracking. As a result, the particle trajectories only represent advection by currents. Ideally, the random-walk process should also be included for the most accurate representation of particle tracking.

In the second part of the numerical experiments, we focused on analyzing the statistical skill of the ETM modeled seven-day forecast performance in simulating all weekly grab samples during the 2018 and 2019 CHAB seasons. We conducted four types of ETM simulations to determine the role of physical transport and biological processes in explaining the short-term variability of MCs and to test the model sensitivity to different initial vertical distributions of MCs. The ETM simulations were designed with two types of initial MC mixing conditions: (1) initializing the ETM by applying MC maps within the surface-mixed layer (referred to as the SML model); and (2) initializing the ETM by applying MC maps throughout the entire water column (referred to as the WC model). Simulations for each mixing condition included two scenarios: one that incorporated microcystin production rates into hydrodynamic transport, and another that did not. In each type of experiment, we conducted 25 individual simulations covering the 2018 and 2019 CHAB seasons. Each simulation ran for 7 days or longer to reach the time point of the subsequent available observation data for model-data comparison (data were from the "HABs Grab" event and GLERL weekly sampling). Occasionally, model simulations were performed for longer than seven days when the GLERL weekly sampling was not sampled on Mondays due to inclement weather.

Model assessment

Model performance was evaluated using confusion matrices. A confusion matrix displays four possible conditions including true positives (TP), true negatives (TN), false positives (FP), and false negatives (FN). Confusion matrices have proven useful for evaluating and communicating model performance in forecasting algal blooms (Anderson et al., 2015; Rowe et al., 2016; Liu et al., 2020; Kim et al., 2021). The model outputs and the observed weekly MC measurements at the eight GLERL sites were compared to several MC threshold values. A ±20% buffer range was

applied to the model output to account for the uncertainty of the ELISA method (Qian et al., 2015) and to avoid being too stringent with the assessment. Each result was defined as correct if the model output and the observed MC concentrations were both above (true positive, ESM Fig. S1a) or both below (true negative, ESM Fig. S1b) the concentration threshold. A false positive occurred when the model output was above the threshold, but the observed MC concentration was below the threshold (ESM Fig. S1c), and a false negative corresponded to the model output being below the threshold but the observed concentration being above it (ESM Fig. S1d). When the model outputs were above (below) the threshold and observed below (above), but the 20% buffer overlapped both the threshold and the observed MC concentrations (ESM Fig. S1e and S1f), the model was considered correct, regarded as true positive (negative). Multiple MC concentration thresholds from different criteria were tested in the skill assessments to examine the model performance in forecasting different ranges of MC concentrations (0.3, 1.0, 5.0, 10.0, and 20.0 μg/L). The 0.3 μg/L level was selected because it is the ELISA method reporting limit (i.e., detectable levels of MC), and 0.3 μg/L is also the Ohio EPA's established drinking water threshold of microcystin concentrations for children under 6 years of age and the group of sensitive individuals. The value of 1 μg/L is the World Health Organization MC guideline for drinking water. The upper range limit of the ELISA test method is 5 μg/L, above which samples require dilutions, and 10 μg/L was selected because it is twice the ELISA range. The threshold that is often used for the public to avoid all contact with the water is 20 μg/L.

The confusion matrix was used to evaluate whether the ETM could capture the observed weekly trend of microcystin concentrations at the eight monitoring sites in the western basin of Lake Erie. This trend was evaluated based on whether the microcystin concentrations increased, decreased, or remained stable from week to week. The model was considered correct if the modeled microcystin concentrations and observed microcystin concentrations changed in the same direction (ESM Fig. S2a, d) or if the ±20% buffer on the modeled concentrations overlapped with both the initial and final observed data (ESM Fig. S2b, e). Conversely, the model was considered incorrect if the model result and observed data showed an opposite trend (ESM Fig. S2c, f). In addition, we also used a “persistence” forecast, which assumes a steady MC pattern over time. The persistence forecast represented the best available information to forecast for a hypothetical scenario if no new data were available. By comparing the ETM with the persistence forecast, we could characterize the quality of the additional information provided by the ETM.

Paired sample T-tests were conducted for the 0.3 μg/L, 1.0 μg/L, and trend analysis across all models to determine if there were significant differences between the years (2018 and 2019), models with and without MC production, and the SML and WC models. Higher concentration thresholds were excluded from this analysis due to the lack of observed MC exceeding 5 μg/L in the 2018 CHAB season.

Results

Observed weekly MC data

The MC concentrations observed in 2019 were generally much higher than those in 2018 (ESM Fig. S3). Despite the concentration differences, the temporal and spatial patterns observed were similar. Both years had low concentrations (<1.0 μg/L) in early July, and the MC levels began to sharply increase in the last week of July. The concentrations peaked during August in both years and then decreased to low levels by late September. In 2018, only one sample exceeded 5 μg/L, whereas in 2019, there were 26 samples above 5 μg/L, including six above 10 μg/L. The sample sites closest to the Maumee River (WE6, 9, 2) had higher concentrations than the sites furthest from shore (WE4 and WE13).

"HABs Grab"

The HABs Grab provided us with a unique opportunity to analyze the impact of hydrodynamic transport and MC production on the spatial variability of MCs in the western basin of Lake Erie, thanks to its sufficiently high spatial resolution and coverage. To discuss the evolution of MCs, we included the latest available MC map (Fig. 2a) from before the HABs Grab and the spatial distribution of MCs during the HABs Grab (Fig. 2b). On July 29th, observations showed that high MC concentrations (2-5 μg/L) originated near the west shore of the western basin and extended to the center of the western basin, with a decrease of MC concentrations to 1-2 μg/L. On the HABs Grab day, the highest MC concentrations (> 20 μg/L) were measured in the region near the mouth of the Maumee River, and concentrations decreased along the south shore with increasing distance to the east. A “finger-shaped” MC plume (1-5 μg/L) was observed in the center of the western basin, pointing to the north shore of the western basin. The "finger" and the high MC concentrations on the west shore of the western basin formed a semi-circular front surrounding the outflow from the mouth of the Detroit River.

A 10-day numerical Lagrangian particle tracking experiment was conducted to identify the impact of hydrodynamic transport on the spatial distribution of MCs. Particles were released in five representative regions, marked in different colors, to reveal how hydrodynamic transport affected their distribution (Fig. 3a). The Detroit River outflow influenced the transport, which first flowed southward in the northern part of the basin and then turned counterclockwise to the northeast to exit the western basin through the passage to the north of Pelee Island (Fig. 3b). Water currents transported particles released in the brown and red rectangles (center and northern areas of the basin, respectively) further east and to the Canadian coast, respectively, corresponding to the “finger" pattern on August 7th. Due to the low current speed at Maumee Bay (Fig. 3b, western corner of the basin), most of the particles released in Maumee Bay (black rectangle) remained in this region, with a small portion of particles moving northward along the western shoreline of the basin. The high residence time in Maumee Bay provided favorable

conditions to accumulate and retain high MC concentration due to MC production in this region. Particles released in the northwest area (purple rectangle) moved slightly southward but were not carried eastward like the particles in the red rectangle, indicating the two close regions belong to two different flow regimes. The movement of particles released in the red and purple regions explained the formation of a steep concentration gradient of MC at 41.70-41.95 degrees latitude and -83.2 degrees longitude. Most of the particles released in the southern area (blue rectangle) stayed inside the blue rectangle due to the low current speed and spread out in all directions according to the horizontal mixing process. One small portion of particles moved northward and joined the extension of the “finger”. Another small portion moved southeastward along the coast, explaining the observed extension of MC along the south coast.

In addition to the Lagrangian particle tracking experiment, the two ETM simulations (with and without MC production) successfully predicted the "finger" and semi-circular shaped front of MCs (Fig. 2c and d). The main difference between the two simulations was the concentration of MCs in Maumee Bay. Only the model with MC production ("WMC") predicted high MC concentrations (> 20 μg/L, Fig. 2c) that were consistent with the observed MC (Fig. 2b). The model without MC production ("WOMC") predicted MC concentrations of less than 5 μg/L in Maumee Bay (Fig. 2d).

Weekly MC forecast skill assessment

Statistical skills were summarized by confusion matrices to evaluate model performance in forecasting different levels of MC concentrations and weekly trends. Each comparison between model-predicted and observed (measured at 8 GLERL sites) MC concentrations in the 2018 and 2019 CHAB seasons was classified into correct (true positive and true negative) and incorrect (false positive and false negative) conditions and marked in corresponding colors (Figs. 4-7). The accuracy was calculated as the ratio of correctly classified events to the total number of events for each case and each site (listed on the X-axis and Y-axis of Figs. 4-7, ESM Figs. S4-S5), and each CHAB season (Table 1 and ESMTable S2). This allowed for a better evaluation of model performance in space and time.

0.3 μg/L threshold

The WC model with MC production (WC-WMC) had the highest accuracy at the 0.3 μg/L thresholds, with 85.4%, 94.2%, and 90.0% in 2018, 2019, and both years combined, respectively (Table 1). The WC-WMC model performed 8.3% to 8.6% better than the SML-WMC model, which involved initializing the model by applying MC concentration maps within the surface mixed layer and simulating MC production. The WC-WOMC model, which did not include microcystin production, was about 10.6% to 20.8% better than the SML-WOMC model. The WMC models outperformed the WOMC models, with a difference of 8.3% to 20.8%. Generally, simulations at sites closer to the Maumee River (Sites WE9, 6, 2, 8, and 12) were more accurate

than those further offshore (Fig. 4). Site WE4, the northernmost site, and more influenced by the Detroit River than the Maumee River (Fig. 1c), had the lowest accuracy within every model simulation (Fig. 4) due to the highly dynamic movement of the HAB front. Across all sites and models, among the incorrect results, there was a general pattern of more false negatives in the early bloom season and more false positives at the end of the year.

1.0 µg/L threshold

In 2018, at the 1.0 µg/L threshold, the persistence model had the highest accuracy (84.4%), which was 9.4% higher than any other model configuration (Table 1). Among the four experiments in 2018, the WC-WOMC model was the second-most accurate (75.0%). The two WMC models (with MC production) generated a combined 14 false positives in July 2018, whereas the two WOMC and persistence models generated only one false positive combined, showing that the WMC models were less accurate in 2018 (a small bloom year) (Fig. 5).

In 2019, which was a big bloom year, the WC-WMC model had the highest accuracy rate of 87.5%, which was 2.9% better than other models (as shown in Table 1). However, the two WOMC and persistence models had lower accuracy rates in 2019 due to generating more false negatives during July and early August compared to the WMC models. During the peak bloom of 2019 (between August 5th and August 19th simulation start times), all models had a high accuracy rate ranging from 75% to 100% for comparison times. However, all models had false positives at the end of the 2019 bloom (on September 3rd and September 24th). There were no apparent spatial patterns in accuracy.

5, 10, and 20 µg/L thresholds

Evaluating higher concentration thresholds for 2018 is complicated by the fact that, except for WE16 on August 20, all other samples had MC concentrations less than 5.0 µg/L (Fig. 6). Throughout the CHAB season, the WOMC and persistence models accurately predicted true negatives for all eight sites, with a 99% accuracy rate. The WC-WMC model, on the other hand, generated 12 false positives, indicating that the model forecast MCs to exceed 5.0 µg/L 12 times, but the observed value was less than 5.0 µg/L (Fig. 6). The SML-WMC model generated only one false positive (Fig. 6).

In 2019, the persistence model had the highest accuracy, but the WC-WMC model's accuracy was only 1% lower than that of the persistence model (Table 1). The SML-WMC model had an accuracy of 83.7% in 2019, while the WC-WMC model had an accuracy of 87.5%, which was

15.4% better than the WOMC counterpart models. However, the SML-WOMC model only correctly predicted 2 out of 35 observations that exceeded 5.0 µg/L, and the WC-WOMC model only correctly predicted 7 out of 35 observations for the 2019 CHAB season. In contrast, the SML-WMC model correctly predicted 20 out of 35 observations that exceeded 5.0 µg/L, which is 57.1%, and the WC-WMC model correctly predicted 26 out of 35 observations, which is 74.3% (Fig. 6).

At the 10 µg/L threshold, the SML-WMC model correctly forecasted that the concentration would exceed 10 µg/L in 5 out of 9 observations. The WC-WMC model correctly forecasted this in 7 out of 9 observations. However, the WOMC models missed every instance of MC exceeding 10 µg/L, and the persistence model only correctly predicted one instance of MC exceeding 10 µg/L (ESM Fig. S4). There were only two instances of MC concentrations that exceeded 20 µg/L, and both WMC models correctly forecasted those instances, while the WOMC models did not (ESM Fig. S5). However, both WMC models generated several false positives for MC concentrations that did not exceed 20 µg/L.

Trend analysis

For trend analysis, the WC-WMC model showed the highest accuracy, achieving 63.5%, 86.5%, and 75.5% in 2018, 2019, and both years combined, respectively. This was between 3.8% and 5.5% better than the next most accurate model, as shown in Table 1. The SML-WMC model, on the other hand, outperformed the SML-WOMC models by 3.2% and 20.2% for 2018 and 2019, respectively. Similarly, the WC-WMC model was 4.1% and 22.1% more accurate than the WC-WOMC models (Table 1).

Across all models (except the persistence model), site WE9, which is the closest site to the Maumee River, had the most correct predictions (76%-80% accuracy). On the other hand, site WE2, located in the transition zone between the nutrient-rich waters of Maumee Bay and the lower-nutrient waters further into the basin, had the lowest accuracy (44%-60%) (Fig. 7a-d). Of particular interest is site WE12, which is located near the City of Toledo's drinking water intake. The WC-WMC model had an overall accuracy of 88%, including 100% accuracy for 2019.

The persistence model would only be correct in trend analysis if observed MC concentrations changed by less than 20% from week to week. However, the persistence model mostly produced false positives and false negatives as shown in Figure 7e. In the latter half of both years, the persistence model had more false negatives due to the declining observed MC concentrations. Overall, the model had an accuracy range of 12% to 36% across all sites, indicating that MC concentrations vary by more than 20% from week to week.

Model scenario comparison

Across all models for the 0.3 µg/L, 1.0 µg/L, and trend analysis, the models had an accuracy of 69.7% (± one standard error of 2.9%) in 2018 and 80.8% (± 2.5%) in 2019 (Fig. 8a). According to the paired sample T-test ($p < 0.001$, $t = -5.358$, $df = 13$), this difference was significant. The models with MC production rate incorporated were significantly more accurate (78.5%) than models without MC production incorporated (69.1%) ($p = 0.002$; $t = 3.934$; $df = 11$; Fig. 8b). Additionally, the WC models (77.3%) were significantly more accurate than SML models (70.3%) ($p = 0.003$; $t = -3.882$; $df = 11$; Fig. 8c).

Discussion

Influences of hydrodynamic transport and MC production on MCs estimation

Our work has revealed that both hydrodynamic transport and MC production are important in predicting MC concentrations. As shown by our "HABs Grab" day simulation, models with MC production agreed with the high MC concentrations observed (>20 µg/L) in Maumee Bay, whereas models without MC production failed to reproduce these high concentrations. Furthermore, all models correctly predicted that water currents would transport the MCs to less commonly affected locations (e.g., northward in Fig. 2c, d), highlighting the importance of hydrodynamic transport of MCs. Our statistical skill assessment over all 2018 and 2019 simulations showed that models without MC production (WOMC) were 69% correct on average, indicating that hydrodynamic transport alone can be used to forecast MC concentrations 7 days into the future. However, incorporating MC production (WMC) rates into the hydrodynamic transport of MCs improved the models by 10%. Additionally, only the models with MC production correctly forecasted MC concentrations greater than 5 µg/L during the large bloom year, but incorrectly forecasted concentrations greater than 5 µg/L (false positives) during the small bloom year. While our study was the first to demonstrate the impact of incorporating biological rates into models on CHAB toxin forecasts, it is important to consider spatial patterns (nearshore vs. offshore), yearly differences (in bloom size), and seasonality (early bloom, peak bloom, and late bloom) when interpreting spatial and temporal modeling results for a large system like western Lake Erie.

Spatial patterns

Site WE9 is located only ~5 km from the Maumee River. While the nutrient concentrations and water temperatures at this site favor cyanobacterial growth, the overall cyanobacterial biovolume can be low compared to other sites (Bridgeman et al., 2013) due to water currents from the

Maumee River preventing the high accumulation of cyanobacteria. During the peak bloom period of 2018, the Maumee Bay area had a low retention time (Chaffin et al., 2021), which resulted in low MC concentrations (ESM Fig. S3) due to flushing. Additionally, in most cases, Maumee River *Microcystis* are not capable of producing microcystins (Kutovaya et al., 2012). In contrast, during the peak bloom in 2019, Maumee Bay had long retention times (Chaffin et al., 2021), allowing MCs to accumulate to high concentrations (up to 45 µg/L, ESM Fig. S3).

Site WE2 is located in the transition zone between the nutrient-rich waters of Maumee Bay and the lower-nutrient waters further into the basin (refer to Fig. 1c). This zone has high nutrient concentrations and more favorable light conditions than the shallow Maumee Bay (less than 2 meters) due to turbidity and increased depth (4-6 meters), which allow for high cyanobacterial growth rates (Chaffin et al., 2011). Site WE2 frequently showed high accuracy in the threshold analyses (Figs. 4-6), but the worst accuracy in the trend analysis, with less than or equal to 60% correct predictions (Fig. 7). The difference can be explained by the consistently high microcystin levels but variable concentrations from week to week at WE2 (ESM Fig. S3). Therefore, MCs were consistently above the thresholds, but the direction of change was more difficult to predict from week to week.

WE12 is important due to its proximity to the City of Toledo's drinking water intake, which is approximately 0.6 km away. The WC-WMC models at this site were accurate, with a correctness rate of at least 88% for all thresholds and trend analyses. Additionally, the models with MC production at WE12 ranked among the top three highest accuracies compared to the other sites. This high accuracy may be attributed to the significant amount of MC data available in a small area around the intake, which was used to initialize the simulations. The City of Toledo collected MC data daily from the intake, while NOAA GLERL, University of Toledo, and charter boats collected samples weekly around the intake. The results at WE12 demonstrate that a higher density of input data can lead to more accurate forecasts.

2018 vs 2019 – low MCs vs high MCs

Much higher MC concentrations (ESM Fig. S3) and cyanobacterial biomass (Chaffin et al., 2021) were observed in the western basin of Lake Erie in 2019 compared to 2018. Across all models for the 0.3 µg/L, 1.0 µg/L, and trend analysis, the high MC year of 2019 had significantly more accurate results than 2018 (Table 1). These results suggest that forecasting MCs may be easier when concentrations are relatively higher when weekly data is available. Severe blooms usually occur in a larger area and last longer, which can be easily captured by weekly observations from a few sites in the western basin. In contrast, small blooms cover a smaller area and have a shorter duration, making them easy to miss when sampling at limited stations. Therefore, ETM performed well in the big bloom year with sufficient data to initialize the model, but failed in the small bloom year.

There were also differences between years regarding models with and without MC production rates. During the low MC year of 2018, the WMC models had more false positives than the WOMC models. For example, at the 1.0 μg/L threshold, the WC-WMC resulted in 26% false positives (25 out of 96 results were false positives), while the WC-WOMC resulted in only 9.4% (9 out of 96) false positives (Fig. 5). On the other hand, during the high MC year of 2019, the WC-WMC model resulted in 5.7% (6 out of 104) false negatives, while the WC-WOMC model resulted in 15.4% (16 out of 104) false negatives. Similar results were observed in the trend analysis. In 2018, the WC-WMC model gave 27.1% (26 out of 96) false positives, whereas the WC-WOMC model gave 8.3% (8 out of 96) false positives. At the 5 μg/L thresholds, the results with and without MC production also differed between the two years, with false positives in the WMC models in 2018 and false negatives in the WOMC models during 2019 (Fig. 6). The false positives in 2018 suggest that our estimate of MC production was too high. We used the average MC production rates reported in microcosms with ambient nutrients and elevated nutrients (Chaffin et al., 2022). The false positives from the WMC models in 2018 may indicate that in situ MC production was closer to that reported in the ambient nutrient treatments than the average of the ambient and elevated nutrient treatments.

Seasonal effect - early bloom, peak bloom, late bloom.

There was a distinct temporal pattern in the results. In early July of both years, all sites had low MCs (< 2 μg/L) and most samples were below detection (0.3 μg/L) or 1.0 μg/L (ESM Fig. S3). MC concentrations increased in late July, remained relatively high (compared to early summer) during August, and then decreased in September. If we apply the general definition of "early bloom" to the first three simulations from early July to mid-July of both years, "peak bloom" to the simulation from late July (starting from July 30th, 2018 or July 29th, 2019) to August, and "late bloom" to the simulations in September, the seasonal patterns become more apparent. In threshold analyses, the models without MC production and the persistence model had more false negatives during the early bloom, especially for 2019, whereas the models with MC production more correctly captured MCs exceeding 0.3 μg/L and 1.0 μg/L during the early bloom, indicating the importance of biological factors in early bloom forecasting (Figs. 4, 5). Across all models, the peak bloom period had the most correct model results compared to the early bloom and late bloom. The late bloom had more false positives than the early bloom at 0.3 μg/L and 1.0 μg/L (apart from the false positives in the WMC 2018 models discussed above).

Microcystins concentrations during the early bloom period were characterized by false negatives in the models without MC production, indicating the challenge for models to capture toxin concentrations during the initiation of the bloom. *Microcystis* overwinters on the lake bottom (Preston et al., 1980; Kitchens et al., 2018) and passively inoculates the water column (via wind resuspension) when water temperature, light, and nutrients allow for growth (Reynolds and Bellinger, 1992; Verspagen et al., 2004). Other models of Lake Erie HABs also struggle to

capture bloom initiation (transition from diatoms to cyanobacteria), which is currently puzzling because there is a lag period between nutrient loading in the spring and the summer occurrence of HABs (Stumpf et al., 2012). For example, the process-based Western Lake Erie Ecosystem Model (WLEEM) factors in hydrology, internal and external nutrient loads, and weather and predicts HAB biovolume, but the model incorrectly initiates the HAB early by up to one month (Verhamme et al., 2016). Recently, the model of Del Giudice et al. (2021) suggested that Lake Erie HABs can initiate one month after the lake has reached 20°C due to a reduction in grazing. Our models relied only on weekly observed MC data, water currents, and measured rates of MC production, and did not account for bloom initiation triggers or benthic recruitment throughout the simulation week. A better understanding of bloom initiation triggers is needed to forecast better when a HAB will begin.

The late bloom period was characterized by false positives, which resulted from decreased observed MC concentrations, but the models forecast an increase in concentration when incorporating the prescribed MC production rates. Cooler water temperatures associated with the late bloom bring about bloom demise as the *Microcystis* colonies settle to the lake bottom (Thomas and Walsby, 1986; Visser et al., 1995; Verspagen et al., 2005). Additionally, cyanophages can infect the *Microcystis* cells in the water column leading to cell lysis and releasing MCs from cells to the aqueous environment (McKindles et al., 2020). Once MCs are outside of the cell, they can be rapidly degraded by heterotrophic bacteria (Mou et al., 2013; Thees et al., 2019). Hence, colony settling and cell lysis followed by MC degradation will decrease MC concentrations. These biological factors were not accounted for in our models, and phage infection and cell lysis were not quantified in the experiments (Chaffin et al., 2022). A better understanding of bloom demise and triggers of cell lysis are needed to inform predictive models better during the late bloom period.

Water column vs surface-mixed layer

In CHAB biomass forecast modeling, several studies have shown that the application of surface chlorophyll concentrations to the surface mixed layer to generate model initial conditions produces the highest accuracy in model simulations (Rowe et al., 2016; Soontiens et al., 2019). Furthermore, Zhou et al. (2023) evaluated multiple models using this approach and confirmed that the ETM performance was the best. However, in our case, the ETM simulation by applying an MC concentration map throughout the entire water column (WC model) as an initial MC condition performed significantly better than SML models, on average, at predicting MC concentrations (Fig. 8).

While there is no consistent relationship between chlorophyll a concentration (or another metric for HAB biomass) and MC concentrations (Stumpf et al., 2016), and most (> 95%) of MCs are intracellular (Dyble et al., 2008; Palagama et al., 2020), it should be expected that MCs and

chlorophyll are positioned similarly in the water column. The differing results between WC vs. SML models for MCs (our study) and chlorophyll (Rowe et al., 2016; Soontiens et al., 2019) are due to the data source used to initialize the simulations. Rowe et al. (2016), Soontiens et al. (2019), and Zhou et al. (2023) used remote sensing surface chlorophyll concentrations. It is dynamically consistent to apply such surface data to the surface mixed layer. Applying surface chlorophyll data to the entire water column would overestimate the water column concentration during surface scums. In addition, the remote-sensed data were available at much higher spatial (300 m) and temporal resolutions (every few days). As a result, the ETM simulation showed close agreement with the observed chlorophyll spatiotemporal pattern (Zhou et al., 2023). Unfortunately, measurements for MC concentrations were much more limited. As we mentioned before, the MC concentration had to be generated by compiling all available data that were measured at different layers of water columns. In this case, applying the initial MC concentration to the entire water column resulted in a relatively better performance.

Therefore, it is critical to understand that the performance of the WC and SML models is affected by how the observed data were collected. Ideally, it would be most appropriate to separate the observational data into near-surface data to be applied to the surface mixed layer and apply the rest of the data to the layer below the surface to generate the initial MC condition. However, this would require a significant amount of data, which is not feasible based on current data availability.

Conclusion

Forecasts of MC concentrations in Lake Erie would be useful for beach managers and drinking water treatment plant operators when making decisions on beach closures and water treatment, respectively. In this study, we developed a novel approach to hindcast MC concentrations for Lake Erie by using a compilation of weekly maps of MC concentrations created from multiple sources of analytical data, a hydrodynamic model, and an Eulerian tracer model. The model results revealed that both hydrodynamic transport and MC production were essential in predicting MC concentrations, which differs from the assumption in CHAB biomass forecasts that physical transport models largely explain the short-term variability of CHAB biomass (Rowe et al., 2016). With very limited data to initialize the ETM, no single model configuration consistently provided more accurate results. Therefore, one must consider all models (with and without MC production, SML vs. WC, including other forecasts developed by other researchers) when making management decisions in an ensemble modeling approach. It is also important to consider the variable performance of different model configurations in different parts of the basin.

The major limitation is that we currently lack accurate, high spatial resolution MC concentration data to initialize ETM. Our model predictions would likely be improved with more accurate initial conditions in 3-D space, as was shown for the HABs Grab. Until recently, the City of

Toledo collected daily MC concentration data, but reduced monitoring to weekly samples to meet changing Ohio EPA compliance requirements. We argue that high-spatial resolution, along with high-temporal sampling frequency, MC data are useful for hindcasting and developing models. These extra daily samples could be stored frozen and analyzed in batches at the end of the CHAB season for research purposes.

Furthermore, our models with MC production were limited by very coarse measurements of MC production (two sites, biweekly). While the models with MC production sometimes overpredicted the MC concentrations and resulted in false positives, especially in 2018, the 10% improvement over models without MC production is a promising result indicating that factoring in biology can improve model forecasts. Likewise, the models would likely be improved by higher temporal and spatial resolution estimates of MC production rate.

Moreover, using a buoyancy regulation model instead of a constant buoyant velocity (90 μm/s) is a potential option to improve our model performance. Medrano et al. (2013) showed that incorporating a buoyancy regulation model can more accurately capture *Microcystis aeruginosa*'s vertical distribution throughout the water column and the diurnal variation in MC concentrations. Furthermore, investigating cell lysis to estimate MC biodegradation rates is another potential option to improve model performance since MC concentrations resulted from the net effect of production and degradation.

In conclusion, our modeling approach, and those of others (Liu et al., 2020, Qian et al., 2021) to MC forecasting, would be improved with more MC observations and a more comprehensive understanding of the biological mechanisms related to MCs through laboratory experiments.

Data and Code Availability

The OSU, UT, and charter boat captain data can be found on NOAA's National Center for Environmental Information (NCEI Accession 0276941), the NOAA GLERL lab data can be found on their website(https://www.glerl.noaa.gov/res/HABs_and_Hypoxia/), and the PWS data can be found by downloading it directly from Ohio EPA (https://epa.ohio.gov/divisions-and-offices/drinking-and-ground-waters/public-water-systems/harmful-algal-blooms). The ETM code and configuration used in this study is available from https://doi.org/10.5281/zenodo.8014770.

Acknowledgments

This is contribution no. 101 of the Great Lakes Research Center at Michigan Technological University. The Michigan Tech high-performance computing cluster, *Superior*, was used in obtaining the modeling results presented in this publication This research was funded by the National Oceanic and Atmospheric Administration's National Centers for Coastal Ocean Science under award NA17NOS4780186 to the Ohio State University. We thank Felix Martinez for

helpful discussion on how to display our model results. This is contribution 1069 from NOAA NCCOS awards.

References

Anderson, E. J., Bechle, A. J., Wu, C. H., Schwab, D. J., Mann, G. E., and Lombardy, K. A. (2015). Reconstruction of a meteotsunami in Lake Erie on 27 May 2012: Roles of atmospheric conditions on hydrodynamic response in enclosed basins. *Journal of Geophysical Research: Oceans,* 120(12), 8020-8038.

Benjamin, S. G., Weygandt, S. S., Brown, J. M., Hu, M., Alexander, C. R., Smirnova, T. G., ... and Manikin, G. S. (2016). A North American hourly assimilation and model forecast cycle: The Rapid Refresh. *Monthly Weather Review*, *144*(4), 1669-1694.

Bridgeman, T. B., Chaffin, J. D., and Filbrun, J. E. (2013). A novel method for tracking western Lake Erie *Microcystis* blooms, 2002–2011. *Journal of Great Lakes Research*, *39*(1), 83-89.

Chaffin, J. D., Bridgeman, T. B., Heckathorn, S. A., and Mishra, S. (2011). Assessment of *Microcystis* growth rate potential and nutrient status across a trophic gradient in western Lake Erie. *Journal of Great Lakes Research*, *37*(1), 92-100.

Chaffin, J. D., Bratton, J. F., Verhamme, E. M., Bair, H. B., Beecher, A. A., Binding, C. E., ... and Zhou, X. (2021). The Lake Erie HABs Grab: A binational collaboration to characterize the western basin cyanobacterial harmful algal blooms at an unprecedented high-resolution spatial scale. *Harmful algae*, *108*, 102080.

Chaffin, J. D., Westrick, J. A., Furr, E., Birbeck, J. A., Reitz, L. A., Stanislawczyk, K., ... and Mayali, X. (2022). Quantification of microcystin production and biodegradation rates in the western basin of Lake Erie. *Limnology and Oceanography*, *67*(7), 1470-1483.

Chen, C., Liu, H., and Beardsley, R. C. (2003). An unstructured grid, finite-volume, three-dimensional, primitive equations ocean model: application to coastal ocean and estuaries. *Journal of atmospheric and oceanic technology*, 20(1), 159-186.

Del Giudice, D., Fang, S., Scavia, D., Davis, T. W., Evans, M. A., and Obenour, D. R. (2021). Elucidating controls on cyanobacteria bloom timing and intensity via Bayesian mechanistic modeling. *Science of the Total Environment*, *755*, 142487.

Den Uyl, P. A., Harrison, S. B., Godwin, C. M., Rowe, M. D., Strickler, J. R., and Vanderploeg, H. A. (2021). Comparative analysis of *Microcystis* buoyancy in western Lake Erie and Saginaw Bay of Lake Huron. *Harmful Algae*, *108*, 102102.

Dyble, J., Fahnenstiel, G. L., Litaker, R. W., Millie, D. F., and Tester, P. A. (2008). Microcystin concentrations and genetic diversity of *Microcystis* in the lower Great Lakes. *Environmental Toxicology: An International Journal*, *23*(4), 507-516.
Golnick, P. C., Chaffin, J. D., Bridgeman, T. B., Zellner, B. C., and Simons, V. E. (2016). A comparison of water sampling and analytical methods in western Lake Erie. *Journal of Great Lakes Research*, *42*(5), 965-971.

Harke, M. J., Steffen, M. M., Gobler, C. J., Otten, T. G., Wilhelm, S. W., Wood, S. A., and Paerl, H. W. (2016). A review of the global ecology, genomics, and biogeography of the toxic cyanobacterium, *Microcystis spp*. *Harmful algae*, *54*, 4-20.

Huang, C., Anderson, E., Liu, Y., Ma, G., Mann, G., and Xue, P. (2021). Evaluating essential processes and forecast requirements for meteotsunami-induced coastal flooding. *Natural Hazards*, 1-26.

Jetoo, S., Grover, V. I., and Krantzberg, G. (2015). The Toledo drinking water advisory: suggested application of the water safety planning approach. *Sustainability*, *7*(8), 9787-9808.

Kane, D. D., Conroy, J. D., Richards, R. P., Baker, D. B., and Culver, D. A. (2014). Re-eutrophication of Lake Erie: Correlations between tributary nutrient loads and phytoplankton biomass. *Journal of Great Lakes Research*, *40*(3), 496-501.

Kim, J. H., Shin, J. K., Lee, H., Lee, D. H., Kang, J. H., Cho, K. H., ... and Park, Y. (2021). Improving the performance of machine learning models for early warning of harmful algal blooms using an adaptive synthetic sampling method. *Water Research*, *207*, 117821.

Kitchens, C. M., Johengen, T. H., and Davis, T. W. (2018). Establishing spatial and temporal patterns in *Microcystis* sediment seed stock viability and their relationship to subsequent bloom development in Western Lake Erie. *PloS one*, *13*(11), e0206821.

Kutovaya, O. A., McKay, R. M. L., Beall, B. F., Wilhelm, S. W., Kane, D. D., Chaffin, J. D., ... and Bullerjahn, G. S. (2012). Evidence against fluvial seeding of recurrent toxic blooms of *Microcystis spp*. in Lake Erie's western basin. *Harmful Algae*, *15*, 71-77.

Li, Y., Chen, X., Chen, C., Ge, J., Ji, R., Tian, R., ... and Xu, L. (2014). Dispersal and survival of chub mackerel (Scomber Japonicus) larvae in the East China Sea. *Ecological Modelling*, *283*, 70-84.

Liu, Q., Rowe, M. D., Anderson, E. J., Stow, C. A., Stumpf, R. P., and Johengen, T. H. (2020). Probabilistic forecast of microcystin toxin using satellite remote sensing, in situ observations and numerical modeling. *Environmental Modelling and Software*, *128*, 104705.

Martin, J. F., Kalcic, M. M., Aloysius, N., Apostel, A. M., Brooker, M. R., Evenson, G., ... and Wang, Y. C. (2021). Evaluating management options to reduce Lake Erie algal blooms using an ensemble of watershed models. Journal of Environmental Management, 280, 111710.

McKindles, K. M., Manes, M. A., DeMarco, J. R., McClure, A., McKay, R. M., Davis, T. W., and Bullerjahn, G. S. (2020). Dissolved microcystin release coincident with lysis of a bloom dominated by *Microcystis spp*. in western Lake Erie attributed to a novel cyanophage. *Applied and environmental microbiology*, *86*(22), e01397-20.

Medrano, E. A., Uittenbogaard, R. E., Pires, L. D., Van De Wiel, B. J. H., and Clercx, H. J. H. (2013). Coupling hydrodynamics and buoyancy regulation in *Microcystis aeruginosa* for its vertical distribution in lakes. *Ecological Modelling*, *248*, 41-56.

Mou, X., Lu, X., Jacob, J., Sun, S., and Heath, R. (2013). Metagenomic identification of bacterioplankton taxa and pathways involved in microcystin degradation in Lake Erie. *PLoS One*, *8*(4), e61890.

Palagama, D. S., Baliu-Rodriguez, D., Snyder, B. K., Thornburg, J. A., Bridgeman, T. B., and Isailovic, D. (2020). Identification and quantification of microcystins in western Lake Erie during 2016 and 2017 harmful algal blooms. *Journal of Great Lakes Research*, *46*(2), 289-301.

Preston, T., Stewart, W. D. P., and Reynolds, C. S. (1980). Bloom-forming cyanobacterium *Microcystis aeruginosa* overwinters on sediment surface. *Nature*, *288*(5789), 365-367

Qian, S. S., Chaffin, J. D., DuFour, M. R., Sherman, J. J., Golnick, P. C., Collier, C. D., ... and Margida, M. G. (2015). Quantifying and reducing uncertainty in estimated microcystin concentrations from the ELISA method. *Environmental science and technology*, *49*(24), 14221-14229.

Qian, S. S., Stow, C. A., Rowland, F. E., Liu, Q., Rowe, M. D., Anderson, E. J., ... and Johengen, T. H. (2021). Chlorophyll a as an indicator of microcystin: Short-term forecasting and risk assessment in Lake Erie. *Ecological Indicators*, *130*, 108055.

Reynolds, C. S., and Bellinger, E. G. (1992). Patterns of abundance and dominance of the phytoplankton of Rostherne Mere, England: evidence from an 18-year data set. *Aquatic Sciences*, *54*, 10-36.

Rowe, M. D., Anderson, E. J., Wynne, T. T., Stumpf, R. P., Fanslow, D. L., Kijanka, K., ... and Davis, T. W. (2016). Vertical distribution of buoyant *Microcystis* blooms in a Lagrangian particle tracking model for short-term forecasts in Lake Erie. *Journal of Geophysical Research: Oceans*, *121*(7), 5296-5314.

Rowe, M. D., Anderson, E. J., Vanderploeg, H. A., Pothoven, S. A., Elgin, A. K., Wang, J., and Yousef, F. (2017). Influence of invasive quagga mussels, phosphorus loads, and climate on spatial and temporal patterns of productivity in Lake Michigan: A biophysical modeling study. *Limnology and Oceanography*, *62*(6), 2629-2649.

Soontiens, N., Binding, C., Fortin, V., Mackay, M., and Rao, Y. R. (2019). Algal bloom transport in Lake Erie using remote sensing and hydrodynamic modelling: sensitivity to buoyancy velocity and initial vertical distribution. *Journal of Great Lakes Research*, *45*(3), 556-572.

Steffen, M. M., Belisle, B. S., Watson, S. B., Boyer, G. L., and Wilhelm, S. W. (2014). Status, causes and controls of cyanobacterial blooms in Lake Erie. *Journal of Great Lakes Research*, *40*(2), 215-225.

Stumpf, R. P., Wynne, T. T., Baker, D. B., and Fahnenstiel, G. L. (2012). Interannual variability of cyanobacterial blooms in Lake Erie.

Stumpf, R. P., Davis, T. W., Wynne, T. T., Graham, J. L., Loftin, K. A., Johengen, T. H., ... and Burtner, A. (2016). Challenges for mapping cyanotoxin patterns from remote sensing of cyanobacteria. *Harmful algae*, *54*, 160-173.

Thees, A., Atari, E., Birbeck, J., Westrick, J. A., and Huntley, J. F. (2019). Isolation and characterization of Lake Erie bacteria that degrade the cyanobacterial microcystin toxin MC-LR. *Journal of Great Lakes Research*, *45*(1), 138-149.

Thomas, R. H., and Walsby, A. E. (1986). The effect of temperature on recovery of buoyancy by *Microcystis*. *Microbiology*, *132*(6), 1665-1672.

Verhamme, E. M., Redder, T. M., Schlea, D. A., Grush, J., Bratton, J. F., and DePinto, J. V. (2016). Development of the Western Lake Erie Ecosystem Model (WLEEM): Application to connect phosphorus loads to cyanobacteria biomass. *Journal of Great Lakes Research*, *42*(6), 1193-1205.

Verspagen, J. M., Snelder, E. O., Visser, P. M., Huisman, J., Mur, L. R., and Ibelings, B. W. (2004). Recruitment of Benthic *Microcystis* (*cyanophyceae*) to the Water Column: Internal Buoyancy Changes or Resuspension? 1. *Journal of Phycology*, *40*(2), 260-270.

Verspagen, J. M., Snelder, E. O., Visser, P. M., Joehnk, K. D., Ibelings, B. W., Mur, L. R., and Huisman, J. E. F. (2005). Benthic–pelagic coupling in the population dynamics of the harmful cyanobacterium *Microcystis*. *Freshwater Biology*, *50*(5), 854-867.

Visser, P. M., Ibelings, B. W., and Mur, L. R. (1995). Autunmal sedimentation of *Microcystis spp*. as result of an increase in carbohydrate ballast at reduced temperature. *Journal of Plankton Research*, *17*(5), 919-933.

Watson, S. B., Miller, C., Arhonditsis, G., Boyer, G. L., Carmichael, W., Charlton, M. N., ... and Wilhelm, S. W. (2016). The re-eutrophication of Lake Erie: Harmful algal blooms and hypoxia. *Harmful algae*, *56*, 44-66.

Wynne, T. T., Stumpf, R. P., Tomlinson, M. C., and Dyble, J. (2010). Characterizing a cyanobacterial bloom in western Lake Erie using satellite imagery and meteorological data. *Limnology and Oceanography*, *55*(5), 2025-2036.

Wynne, T. T., Stumpf, R. P., Tomlinson, M. C., Fahnenstiel, G. L., Dyble, J., Schwab, D. J., and Joshi, S. J. (2013). Evolution of a cyanobacterial bloom forecast system in western Lake Erie: development and initial evaluation. *Journal of Great Lakes Research*, *39*, 90-99.

Xue, P., Eltahir, E. A., Malanotte-Rizzoli, P., and Wei, J. (2014). Local feedback mechanisms of the shallow water region around the Maritime Continent. *Journal of Geophysical Research: Oceans*, 119(10), 6933-6951.

Xue, P., Schwab, D. J., and Hu, S. (2015). An investigation of the thermal response to meteorological forcing in a hydrodynamic model of Lake Superior. *Journal of Geophysical Research: Oceans,* 120(7), 5233-5253.

Xue, P., Pal, J. S., Ye, X., Lenters, J. D., Huang, C., and Chu, P. Y. (2017). Improving the simulation of large lakes in regional climate modeling: Two-way Lake–atmosphere coupling with a 3D hydrodynamic model of the Great Lakes. *Journal of Climate*, *30*(5), 1605-1627.

Xue, P., Ye, X., Pal, J. S., Chu, P. Y., Kayastha, M. B., and Huang, C. (2022). Climate projections over the Great Lakes Region: using two-way coupling of a regional climate model with a 3-D lake model. *Geoscientific Model Development*, *15*(11), 4425.

Zhou, X., Auer, M. T., and Xue, P. (2021). Open Lake Phosphorus Forcing of *Cladophora* Growth: Modeling the Dual Challenge in Great Lakes Trophic State Management. *Water*, 13(19), 2680.

Zhou, X., Rowe, M., Liu, Q., and Xue, P. (2023). Comparison of Eulerian and Lagrangian transport models for harmful algal bloom forecasts in Lake Erie. *Environmental Modelling and Software*, 162, 105641.

Table 1. The accuracy of the four experiments and persistence model for the 2018 and 2019 season at the 0.3 µg/L, 1.0 µg/L, and 5.0 µg/L microcystin concentrations thresholds and the trend analysis. The model with the highest accuracy is bolded and underlined. SML = initial microcystins were mixed within the surface mixed layer for the initial conditions; WC = initial microcystins were mixed throughout the entire water column; WMC = ETM simulations with microcystin production; WOMC = ETM simulations without microcystin production.

Threshold	Year	SML-WMC	SML-WOMC	WC-WMC	WC-WOMC	Persistence model
0.3 µg/L	2018	77.1%	56.3%	**85.4%**	77.1%	79.2%
	2019	85.6%	75.0%	**94.2%**	85.6%	89.4%
	Both years	81.5%	66.0%	**90.0%**	81.5%	84.5%
1.0 µg/L	2018	74.0%	67.7%	67.7%	75.0%	**84.4%**
	2019	81.7%	71.2%	**87.5%**	80.8%	84.6%
	Both years	78.0%	69.5%	78.0%	78.0%	**84.5%**
5.0 µg/L	2018	97.9%	**99.0%**	86.5%	**99.0%**	**99.0%**

Figure Captions:

Fig. 1. (a) An example of a microcystin concentration map (August 19th, 2019) for the western basin of Lake Erie. (b) The sample collection locations of the HABs Grab on August 19th, 2019. (c) The weekly sample locations by GLERL. (d) An enlarged view of the ETM grid (in red) in the western basin of Lake Erie with blue triangles marking the sampling locations used to collect water for microcystin production experiments (Chaffin et al., 2022). The solid black line distinguishes the areas within 20 km of the Maumee River mouth from the rest of the basin.

Fig. 2. (a) An MC concentration map generated from multiple MC data sources for July 29th, 2019. July 29th is the latest available observation prior to the HABs Grab on August 7th, 2019. This MC concentration map was used to initialize the ETM simulation (b) An MC concentration map generated based on the observation data from HABs Grab. Black dots on the maps ([a] and [b]) represent the sampling locations on those days, respectively. (c) and (d): Simulated average MC concentrations from the surface to 2m depth on the HABs Grab day from the ETM with MC production (WMC, panel c) and without MC production (WOMC, panel d).

Fig. 3. (a) Trajectories of fluid particles released from five representative regions (marked in different colors) over the MC map on July 29th, 2019 (Fig. 2a) to show the impact of hydrodynamic transport on the spatial distribution of MCs. (b) 10-day mean depth-averaged flow field from July 29th to August 7th, 2019 simulated with LE-FVCOM.

Fig. 4. Summary confusion matrix of the model assessment at the 0.3 μg/L thresholds. Dark blue = model was correct (true positive) in that both the output and observed microcystin concentrations were above 0.3 μg/L, or the model output was above the threshold and observed below, but the 20% buffer overlapped both the threshold and the observed MC concentration. Light blue = model was correct (true negative) in that both the output and observed microcystin concentrations were below 0.3 μg/L. Dark gray = model was incorrect (false positive) in that the model was above 0.3 μg/L while the observed was below. White = model was incorrect (false negative) in that the model output was below 0.3 μg/L but observed was greater. The percentages listed on the X-axis and Y-axis are the accuracy (dark and light blue grids) for each date (across all sites) and each site (across all dates). The Y-axis is arranged from the site farthest from the Maumee River (WE16) to the closest (WE9).

Fig. 5. As Fig. 4 caption, but at the 1.0 μg/L threshold.

Fig. 6. As Fig. 4 caption, but at the 5.0 μg/L threshold.

Fig. 7. Summary confusion matrix of the model assessment for the trend analysis. For the ETM simulation (SML-WMC, SML-WOMC, WC-WMC, WC-WOMC), Dark blue = model was correct (true positive) in that both the output and observed microcystin concentrations increased.

Light blue = model was correct (true negative) in that both the output and observed microcystin concentrations decreased. Purple = MC concentrations on the simulation start date and final were within 20%, indicating no increase or decrease within the allowed buffer, and the model was considered correct. Dark gray = model was incorrect (false positive) in that the model increased microcystin concentration while observed decreased. White = model was incorrect (false negative) in that the model decreased microcystin concentration, but the observed concentration increased. For the persistence model, the purple color showed the observed data changed less than 20% from the previously observed data (correct), the dark gray showed the observed data increased more than 20% from the previously observed data (false positive), and the white showed the observed data decreased more than 20% from the previously observed data (false negative). The percentages listed on the X-axis and Y-axis are the accuracy (dark and light blue grids) for each date (across all sites) and each site (across all dates). The Y-axis is arranged from the site furthest from the Maumee River (WE16) to the closest (WE9).

Fig. 8. Average accuracy (± one standard error) for all models in the 0.3 μg/L, 1.0 μg/L, and the trend analysis for (A) 2018 and 2019, (B) with and without microcystin production rates, (C) and water column mixing scenario.

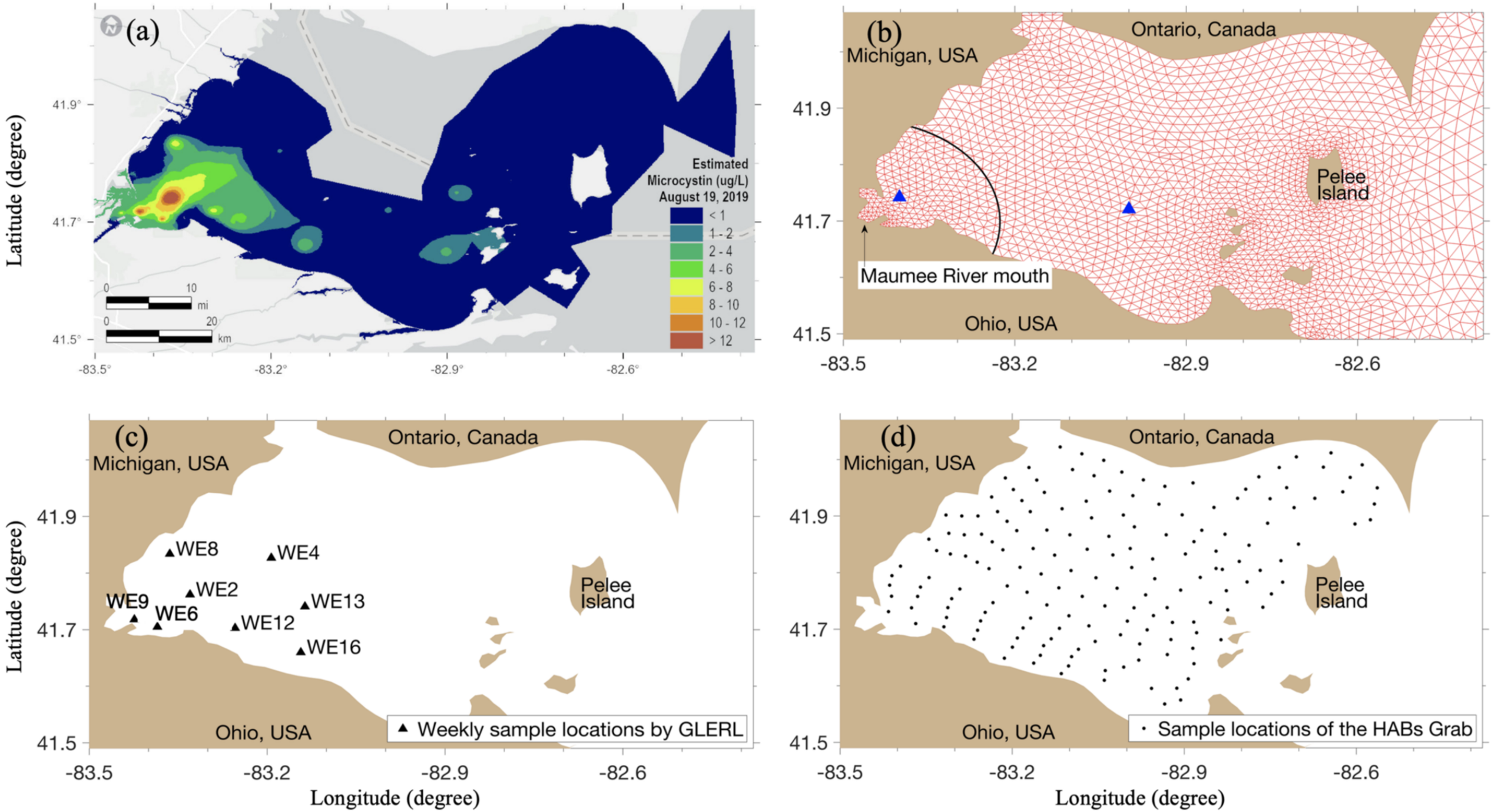
(a)
Estimated
Microcystin (ug/L)
August 19, 2019
< 1
1 - 2
2 - 4
4 - 6
6 - 8
8 - 10
10 - 12
> 12
0 10 mi
0 20 km
41.9°
41.7°
41.5°
-83.5°
-83.2°
-82.9°
-82.6°
Latitude (degree)
(b)
Michigan, USA
Ontario, Canada
Ohio, USA
Pelee Island
Maumee River mouth
41.9
41.7
41.5
-83.5
-83.2
-82.9
-82.6
(c)
Michigan, USA
Ontario, Canada
Ohio, USA
Pelee Island
WE8
WE4
WE2
WE9
WE6
WE12
WE13
WE16
Weekly sample locations by GLERL
Latitude (degree)
Longitude (degree)
(d)
Michigan, USA
Ontario, Canada
Ohio, USA
Pelee Island
Sample locations of the HABs Grab
Longitude (degree)

Microcystin (μg/L)

0 0.3 1 2 5 10 15 20 30 40 50

(a) Ontario, Canada
Michigan, USA
Pelee Island
Ohio, USA

(b) Ontario, Canada
Michigan, USA
Pelee Island
Ohio, USA

WMC

WOMC

(c) Ontario, Canada
Michigan, USA
Pelee Island
Ohio, USA

(d) Ontario, Canada
Michigan, USA
Pelee Island
Ohio, USA

Latitude (degree)
41.9
41.7
41.5

-83.5 -83.2 -82.9 -82.6

Longitude (degree)

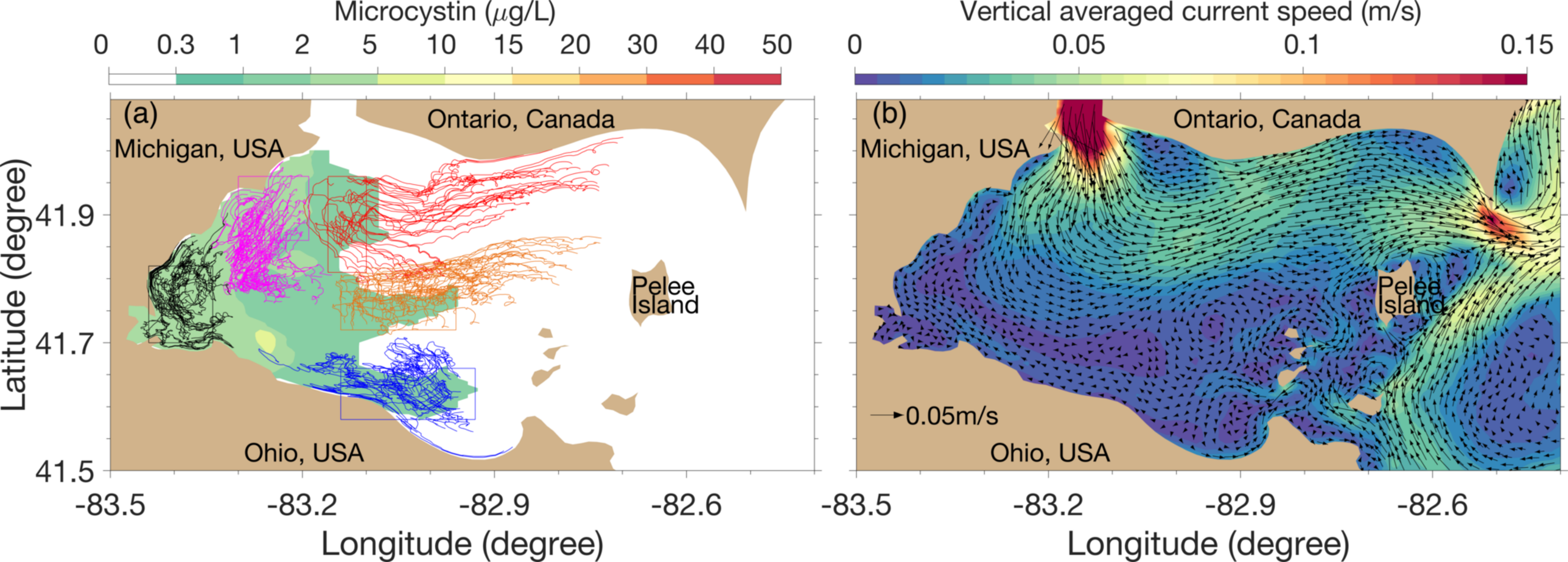
Microcystin (μg/L)
0
0.3
1
2
5
10
15
20
30
40
50
Vertical averaged current speed (m/s)
0
0.05
0.1
0.15
(a)
Ontario, Canada
Michigan, USA
Pelee Island
Ohio, USA
(b)
Ontario, Canada
Michigan, USA
Pelee Island
0.05m/s
Ohio, USA
Latitude (degree)
41.9
41.7
41.5
-83.5
-83.2
-82.9
-82.6
Longitude (degree)
Longitude (degree)

Correct (true positive), modeled and observed MCs both above threshold, or 20% buffer overlapped
Correct (true negative), model and observed MCs both below threshold
Incorrect (false positive), modeled MCs above threshold but observed below
Incorrect (false negative), modeled MCs below threshold but observed above

SML-WMC (a)

WE16 (76%) 62% 62% 75% 88% 62% 100% 88% 88% 88% 100% 88% 25% 100% 88% 88% 75% 100% 100% 100% 100% 88% 62% 88% 25% 100%
WE13 (80%)
WE4 (56%)
WE12 (84%)
WE8 (92%)
WE2 (84%)
WE6 (92%)
WE9 (88%)

SML-WOMC (b)

WE16 (60%) 62% 50% 38% 12% 38% 62% 62% 88% 88% 100% 50% 25% 100% 62% 12% 75% 100% 100% 100% 100% 88% 25% 88% 25% 100%
WE13 (64%)
WE4 (52%)
WE12 (68%)
WE8 (76%)
WE2 (60%)
WE6 (68%)
WE9 (80%)

WC-WMC (c)

GLERL sites

WE16 (88%) 75% 75% 75% 100% 100% 100% 88% 88% 100% 100% 88% 38% 100% 88% 88% 88% 100% 100% 100% 88% 88% 100% 88% 100% 100%
WE13 (88%)
WE4 (72%)
WE12 (96%)
WE8 (92%)
WE2 (96%)
WE6 (96%)
WE9 (92%)

WC-WOMC (d)

WE16 (76%) 62% 50% 75% 62% 75% 88% 88% 88% 100% 100% 88% 50% 100% 62% 12% 75% 100% 100% 100% 100% 88% 88% 88% 100% 100%
WE13 (80%)
WE4 (68%)
WE12 (92%)
WE8 (84%)
WE2 (76%)
WE6 (84%)
WE9 (92%)

Persistence Model (e)

WE16 (88%) 07/05 to 07/09 (62%) 07/09 to 07/16 (38%) 07/16 to 07/23 (88%) 07/23 to 07/30 (88%) 07/30 to 08/06 (88%) 08/02 to 08/06 (88%) 08/06 to 08/13 (100%) 08/09 to 08/13 (100%) 08/13 to 08/20 (100%) 08/27 to 09/04 (88%) 09/04 to 09/11 (88%) 09/11 to 09/17 (25%) 07/02 to 07/08 (100%) 07/08 to 07/15 (62%) 07/15 to 07/22 (50%) 07/22 to 07/29 (88%) 07/28 to 07/29 (88%) 07/28 to 08/05 (100%) 07/29 to 08/05 (100%) 08/07 to 08/12 (88%) 08/12 to 08/19 (88%) 08/19 to 08/28 (100%) 08/28 to 09/03 (100%) 09/06 to 09/16 (100%) 09/16 to 09/24 (100%)
WE13 (84%)
WE4 (72%)
WE12 (88%)
WE8 (84%)
WE2 (88%)
WE6 (88%)
WE9 (84%)

2018 2019

Model start time to the model-observation compare time

Correct (true positive), modeled and observed MCs both above threshold, or 20% buffer overlapped
Correct (true negative), model and observed MCs both below threshold
Incorrect (false positive), modeled MCs above threshold but observed below
Incorrect (false negative), modeled MCs below threshold but observed above

SML-WMC (a)

WE16 (76%) 100% 50% 75% 50% 62% 88% 100% 62% 62% 75% 75% 88% 100% 62% 75% 75% 100% 100% 100% 100% 100% 25% 62% 62% 100%
WE13 (84%)
WE4 (80%)
WE12 (84%)
WE8 (72%)
WE2 (76%)
WE6 (80%)
WE9 (72%)

SML-WOMC (b)

WE16 (52%) 100% 75% 100% 50% 25% 88% 38% 62% 25% 50% 100% 100% 100% 88% 38% 38% 100% 88% 75% 100% 75% 0% 62% 62% 100%
WE13 (88%)
WE4 (72%)
WE12 (68%)
WE8 (64%)
WE2 (72%)
WE6 (72%)
WE9 (68%)

WC-WMC (c)

GLERL sites

WE16 (76%) 100% 50% 38% 75% 75% 88% 88% 75% 75% 75% 25% 50% 100% 75% 75% 75% 100% 100% 100% 88% 100% 75% 50% 100% 100%
WE13 (64%)
WE4 (76%)
WE12 (88%)
WE8 (84%)
WE2 (80%)
WE6 (88%)
WE9 (68%)

WC-WOMC (d)

WE16 (68%) 100% 62% 100% 50% 62% 88% 75% 88% 88% 62% 50% 75% 100% 88% 38% 50% 100% 100% 88% 88% 88% 62% 50% 100% 100%
WE13 (84%)
WE4 (80%)
WE12 (76%)
WE8 (88%)
WE2 (72%)
WE6 (80%)
WE9 (76%)

Persistence Model (e)

WE16 (84%) 07/05 to 07/09 (100%) 07/09 to 07/16 (75%) 07/16 to 07/23 (100%) 07/23 to 07/30 (75%) 07/30 to 08/06 (88%) 08/02 to 08/06 (88%) 08/06 to 08/13 (100%) 08/09 to 08/13 (100%) 08/13 to 08/20 (75%) 08/27 to 09/04 (88%) 09/04 to 09/11 (25%) 09/11 to 09/17 (100%) 07/02 to 07/08 (100%) 07/08 to 07/15 (88%) 07/15 to 07/22 (50%) 07/22 to 07/29 (62%) 07/28 to 07/29 (62%) 07/28 to 08/05 (100%) 07/29 to 08/05 (100%) 08/07 to 08/12 (75%) 08/12 to 08/19 (100%) 08/19 to 08/28 (100%) 08/28 to 09/03 (62%) 09/06 to 09/16 (100%) 09/16 to 09/24 (100%)
WE13 (88%)
WE4 (84%)
WE12 (84%)
WE8 (88%)
WE2 (84%)
WE6 (92%)
WE9 (72%)

2018 2019

Model start time to the model-observation compare time

Correct (true positive), modeled and observed MCs both above threshold, or 20% buffer overlapped
Correct (true negative), model and observed MCs both below threshold
Incorrect (false positive), modeled MCs above threshold but observed below
Incorrect (false negative), modeled MCs below threshold but observed above

SML-WMC (a)

WE16 (96%) 100% 100% 100% 100% 100% 100% 88% 100% 88% 100% 100% 100% 100% 100% 62% 88% 50% 88% 100% 75% 62% 75% 88% 100% 100%
WE13 (96%)
WE4 (96%)
WE12 (88%)
WE8 (84%)
WE2 (88%)
WE6 (84%)
WE9 (92%)

SML-WOMC (b)

WE16 (96%) 100% 100% 100% 100% 100% 100% 100% 100% 88% 100% 100% 100% 100% 100% 62% 38% 38% 38% 38% 50% 62% 75% 88% 100% 100%
WE13 (100%)
WE4 (92%)
WE12 (76%)
WE8 (72%)
WE2 (76%)
WE6 (68%)
WE9 (84%)

WC-WMC (c)

GLERL sites

WE16 (84%) 100% 75% 100% 100% 62% 100% 62% 100% 88% 75% 75% 100% 100% 100% 62% 88% 75% 88% 100% 75% 88% 75% 88% 100% 100%
WE13 (92%)
WE4 (100%)
WE12 (96%)
WE8 (84%)
WE2 (88%)
WE6 (76%)
WE9 (76%)

WC-WOMC (d)

WE16 (96%) 100% 100% 100% 100% 100% 100% 100% 100% 88% 100% 100% 100% 100% 100% 62% 38% 38% 38% 38% 88% 75% 75% 88% 100% 100%
WE13 (100%)
WE4 (92%)
WE12 (80%)
WE8 (80%)
WE2 (72%)
WE6 (72%)
WE9 (88%)

Persistence Model (e)

WE16 (96%) 07/05 to 07/09 (100%) 07/09 to 07/16 (100%) 07/16 to 07/23 (100%) 07/23 to 07/30 (100%) 07/30 to 08/06 (100%) 08/02 to 08/06 (100%) 08/06 to 08/13 (100%) 08/09 to 08/13 (100%) 08/13 to 08/20 (88%) 08/27 to 09/04 (100%) 09/04 to 09/11 (100%) 09/11 to 09/17 (100%) 07/02 to 07/08 (100%) 07/08 to 07/15 (100%) 07/15 to 07/22 (62%) 07/22 to 07/29 (75%) 07/28 to 07/29 (75%) 07/28 to 08/05 (88%) 07/29 to 08/05 (88%) 08/07 to 08/12 (88%) 08/12 to 08/19 (100%) 08/19 to 08/28 (75%) 08/28 to 09/03 (100%) 09/06 to 09/16 (100%) 09/16 to 09/24 (100%)
WE13 (100%)
WE4 (92%)
WE12 (92%)
WE8 (92%)
WE2 (88%)
WE6 (96%)
WE9 (92%)

2018 2019

Model start time to the model-observation compare time

legend for SML-WMC, SML-WOMC, WC-WMC, WC-WOMC

- Correct (true positive), both modeled and observed MCs increased
- Correct (true negative), both model and observed MCs decreased
- Correct, ±20% buffer on the modeled MCs overlapped with observed data
- Incorrect (false positive), modeled MCs increased but observed decreased
- Incorrect (false negative), modeled MCs decreased but observed increased

legend for Persistence Model

- Correct, the observed MCs changed less than 20% from the previous observation
- Incorrect (false positive),the observed MCs increased more than 20% from the previous observation
- Incorrect (false negative), the observed MCs decreased more than 20% from the previous observation

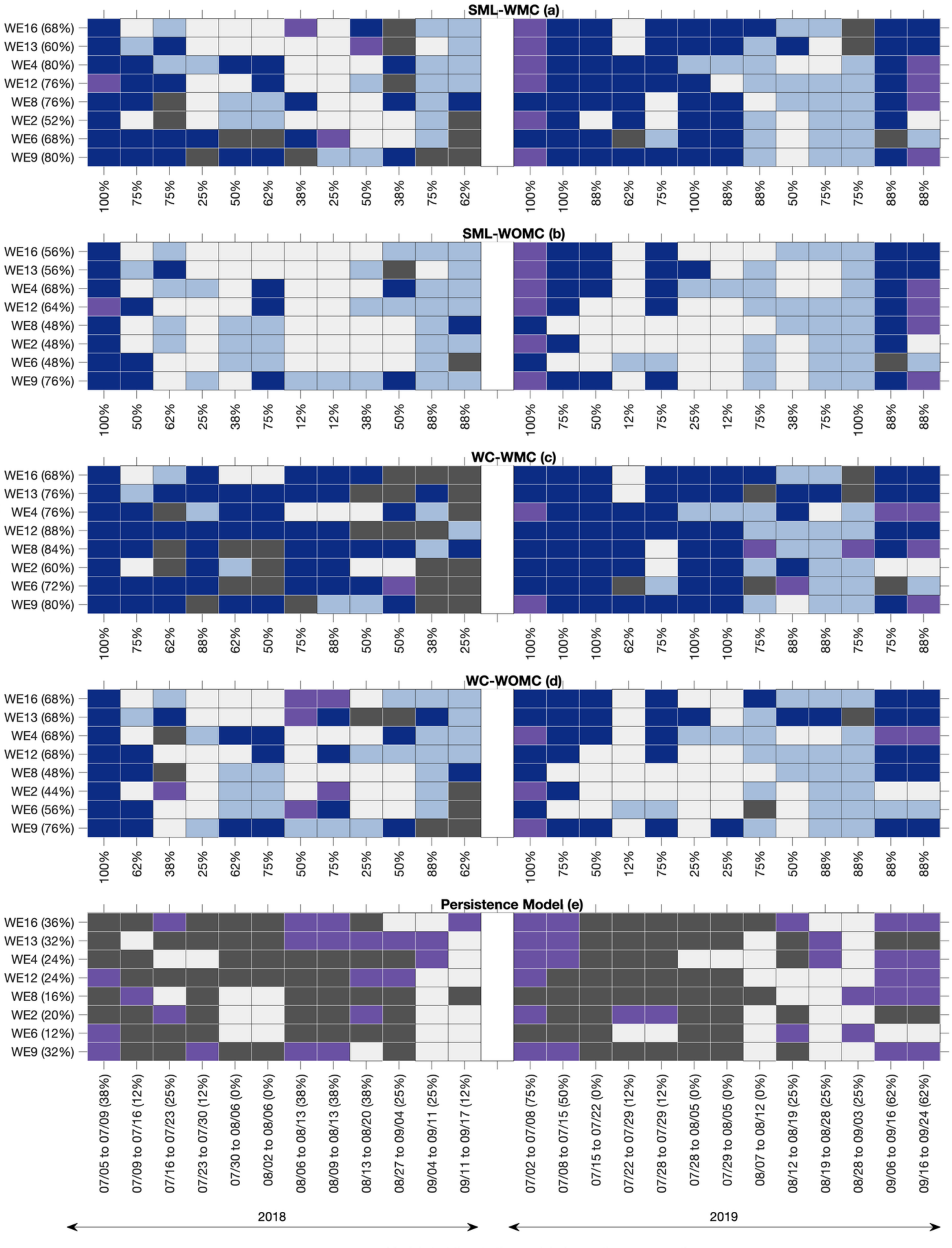

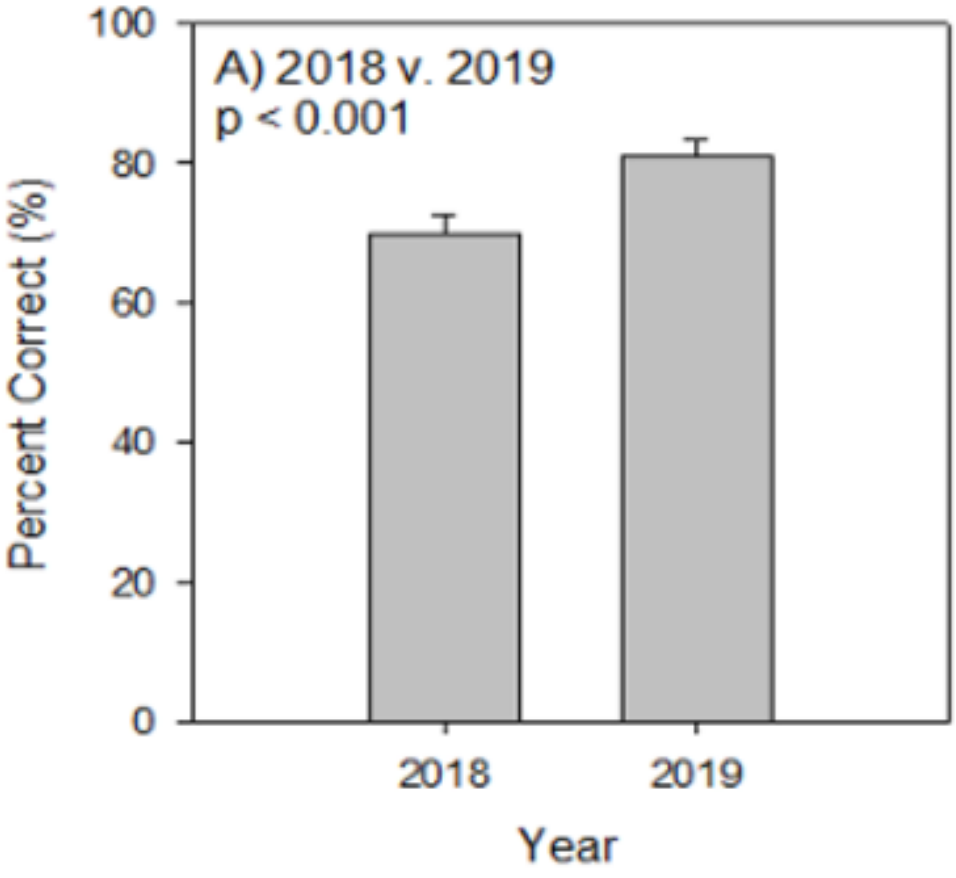
A) 2018 v. 2019
p < 0.001
Percent Correct (%)
100
80
60
40
20
0
2018
2019
Year

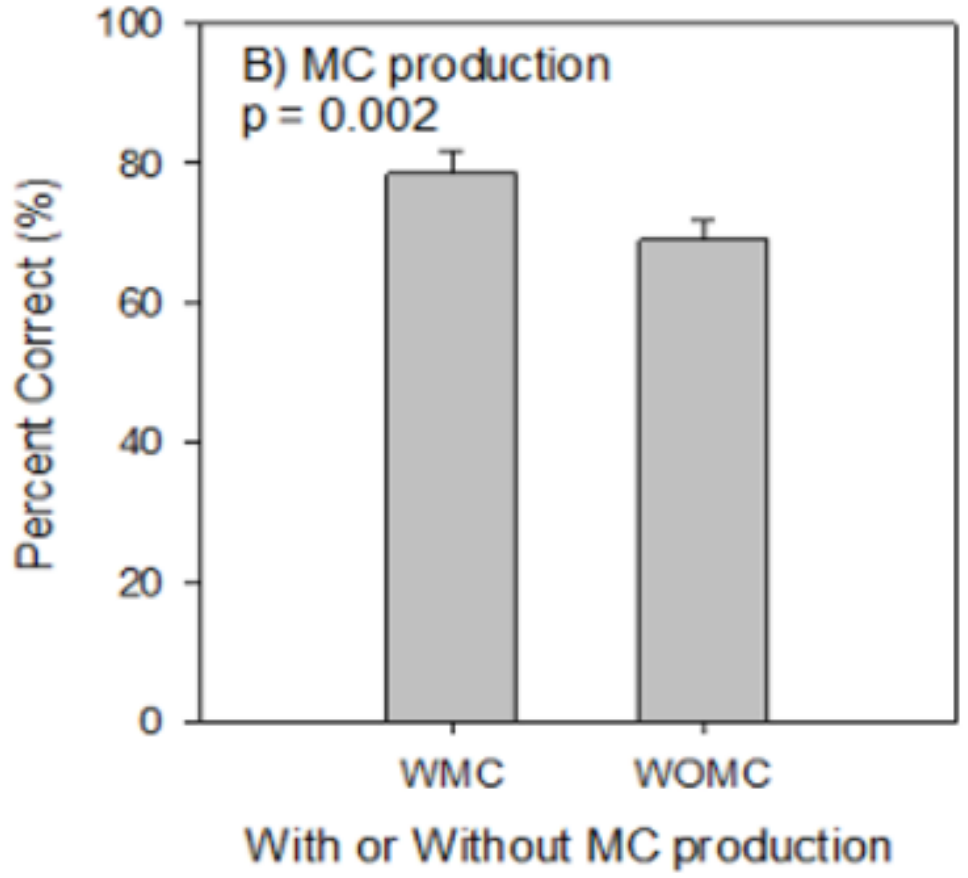
B) MC production
p = 0.002
Percent Correct (%)
100
80
60
40
20
0
WMC
WOMC
With or Without MC production

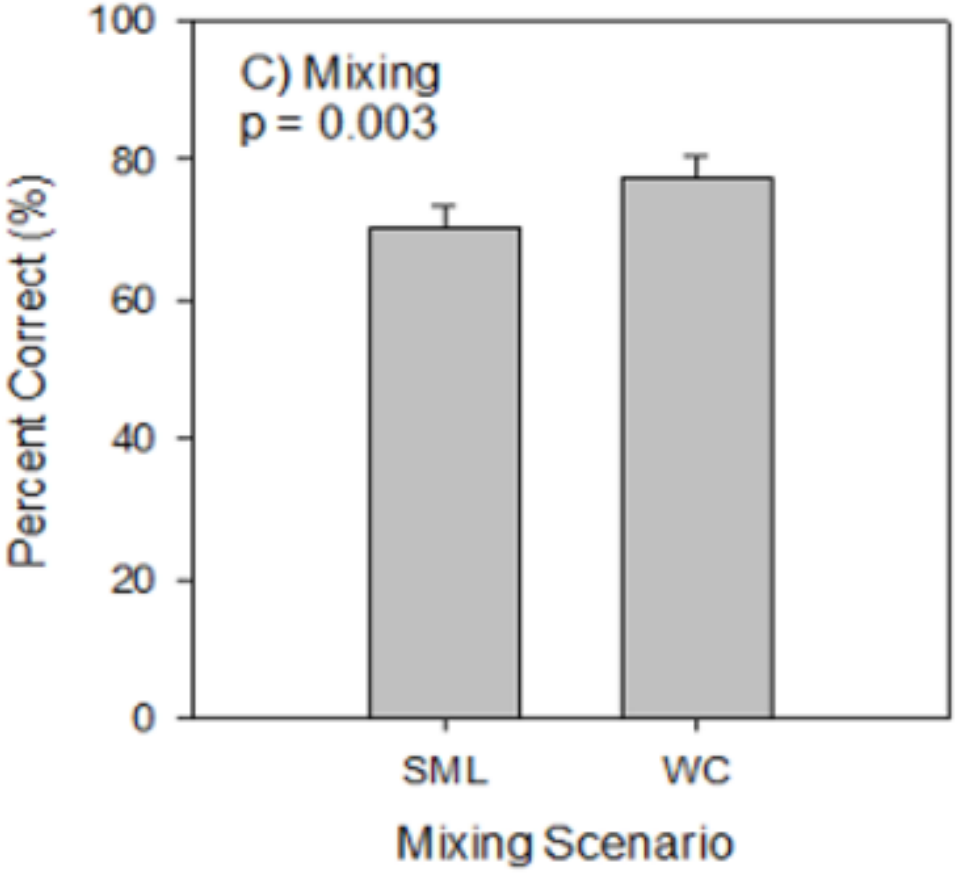
C) Mixing
p = 0.003
Percent Correct (%)
100
80
60
40
20
0
SML
WC
Mixing Scenario